Arm Retraction Dynamics and Bistability of a Three-Arm Star Polymer in a Nanopore

ARTICLE *in* MACROMOLECULES · MARCH 2014

Impact Factor: 5.8 · DOI: 10.1021/ma500053n

3 AUTHORS, INCLUDING:

Andrey Milchev
Bulgarian Academy of Sciences
237 PUBLICATIONS **4,464** CITATIONS
SEE PROFILE

Marcus Müller
Georg-August-Universität Göttingen
341 PUBLICATIONS **10,228** CITATIONS
SEE PROFILE

Macromolecules

Article

pubs.acs.org/Macromolecules

Arm Retraction Dynamics and Bistability of a Three-Arm Star Polymer in a Nanopore

A. Milchev,*[,†,‡] M. Müller,[‡] and L. Klushin[§]

[†]Institute for Physical Chemistry, Bulgarian Academy of Sciences, 1113 Sofia, Bulgaria

[‡]Institut für Theoretische Physik, Friedrich-Hund-Platz 1, 37077 Göttingen, Germany

[§]Department of Physics, American University of Beirut, Beirut, Lebanon

ABSTRACT: Using molecular dynamics and Monte Carlo simulations as well as analytical considerations, we study the arm-retraction dynamics of a three-arm star polymer in a narrow nanotube as a function of arm length, N, and tube diameter, D. The system dynamics is analyzed and compared to the bistable collective behavior of a pair of polymer chains tethered in a nanopore. The bistability arises from alternate flipping of one arm of the star into the pore section occupied to that moment by a single arm only. We derive analytical expressions for the free-energy landscape of an arm flip and determine the barrier height as a function of N and D. In the related case of two chains in a narrow tube, we demonstrate that correlations lead to a *bimodal* distribution of the chain-end positions whereas in a polymer brush, made of equivalent chains at the same grafting density, one observes a single peak only. The residence time distribution between consecutive arm flips is shown to follow a power-exponential relationship, demonstrating good agreement between theory and simulation.

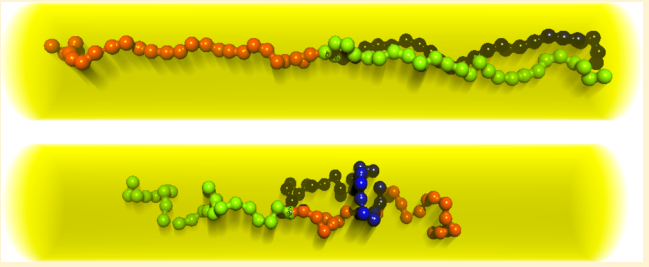

I. INTRODUCTION

Star-shaped polymers constitute an important class of polymers with nonlinear branched architecture that is representative of soft colloids bridging the gap between hard spheres and polymers.[1] These macromolecular aggregates of f linear, flexible polymer chains, which are chemically linked to a common core, are technologically important for a variety of applications ranging from viscosity modifiers in the oil industry[2] to, most notably, novel drug-delivery agents.[3−5] Over the last 3 decades, star polymers have been subject of abiding experimental[6−12] and theoretical[13−15] studies, mainly focusing on their rheological properties in melts and solutions or in mixtures with linear polymers. A prominent result of these studies was the development of a microscopic theory of stress relaxation in star polymer melts, based on the concept of arm retraction,[13,14,16] that is in remarkably good agreement to rheological data on star polymer melts. A large number of computer simulation studies[17−27] has provided valuable information and tests of the theoretical models in this field.

Comparatively less studied, however, has remained the behavior of star polymers in confinement. Theoretical investigations[28,29] and computer simulations[30−35] examined the behavior of star polymers in a narrow slit. The properties of a star polymer in a narrow cylindrical tube, to the best of our knowledge, have not been investigated so far, albeit the flow injection of branched polymers inside nanopores was been theoretically considered by Sakaue et al.,[36] whereas Ge et al.[37] experimentally studied the ultrafiltration of star-like polystyrene molecules with different arm lengths, N, and arm numbers, (i.e., functionality) f, passing through a nanopore.

In the present work we theoretically investigate the dynamics of star polymers in a narrow cylindrical pore and compare predictions of scaling theory to data obtained from molecular dynamics (MD) and Monte Carlo simulations of such branched macromolecules. We show that the conformational relaxation of star polymers in cylindrical confinement is driven by an arm-retraction mechanism whereby, in the simplest case of three-arm stars, this conformational dynamics is closely related to the bistable behavior of the arms in the nanopore. Such bistable nanomechanical elements on the basis of confined tethered polymers have recently been investigated by Zhang et al.[38] and Osmanovic et al.[39] In the case of confined stars, bistability arises due to the presence of two, entropically favorable states when one side of the pore (with respect to the core monomer) is occupied by one arm only whereas the remaining two arms fill the opposite side of the pore. Such overlap of two self-avoiding polymers in a cylindrical confinement leads to entropic segregation and is known to have, e.g., important implications for chromosome segregation in bacterial cells.[40−43]

Our manuscript is arranged as follows: In section II, we establish an approximate, analytical expression for the free energy of such a bistable system based upon scaling arguments. In addition to the geometrically confined three-arm star polymer, we also study a pair of linear chains, tethered to the capped bottom of a nanopore. This case mimics the behavior of

Received: January 7, 2014
Revised: February 16, 2014

   dx.doi.org/10.1021/ma500053n | *Macromolecules* XXXX, XXX, XXX−XXX

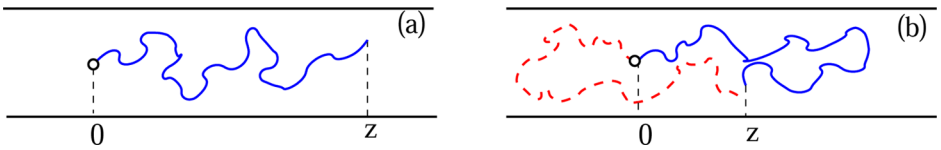

Figure 1. Sketch of a chain in a narrow tube with an end-to-end distance z: (a) uniform, stretched conformation; (b) conformation with a hairpin.

two arms on the same side of the star core and it is also related to the behavior of a polymer brush. The probability distribution of chain-end positions along a capped nanopore is bimodal, corresponding to partial shrinking of one, and stretching of the other of the two chains. In section III, we introduce our computational model and simulation techniques. Then, section IV details our simulation results and compares them to the theoretical description. The free energy barrier for the exchange of chain-end positions agrees with the analytical considerations, and we examine the dynamic behavior of a three-arm star in a nanotube, focusing on the dependence of the free-energy barrier on arm length N and tube diameter D. We demonstrate that the time for a star arm to change sides with the core follows a power-exponential law in agreement with the analytical considerations. The manuscript concludes with a brief discussion in section V.

II. BACKGROUND: SCALING CONSIDERATIONS

A. A Single Chain Tethered Inside a Tube. Arm retraction involves the formation of a hairpin bend in order to change the arm orientation. In a star polymer, the picture is more intricate since the other arms adjust to the configuration of the retracting one. A simpler but conceptually very similar situation takes place when one linear chain comprised of N monomers end-tethered to a point, $z = 0$, on the axis of a tube, see Figure 1a, switches from one side of the tethering anchor to the opposite one.

We are interested in the free energy of a flexible chain, grafted with one end at $z = 0$ inside a narrow tube, as a function of the position, z, of the opposite end. This Landau free energy, $F(z)$, is related to the probability density $P(z)$ of finding the chain end at position z via $F(z) = -k_BT \ln P(z)$. In the limit of a narrow tube, the unconfined macromolecular extension $R = aN^{\nu}$ is much larger than the tube diameter D. N denotes the number of segments of the chain, a the segment length, and $\nu \approx 0.588$ is the scaling exponent of a self-avoiding random walk. For $R \gg D$, one envisions the macromolecular conformation as a linear string of blobs of spatial extension D. The number of segments per blob scales like $D^{1/\nu}$ and the entire macromolecule is comprised of $ND^{-1/\nu}$ blobs. The free-energy minimum is attained when this string of blobs fully extends either to the right or to the left of the grafting point. This is a prototypical example of a bistable equilibrium with two equilibrium positions at $z = \pm l_z^{eq}$, where $l_z^{eq} \propto ND^{1-(1/\nu)}$ is the longitudinal size of the chain in the tube. If the free end only slightly moves toward the grafting point, the chain of blobs will become weakly compressed but will remain a linear string and the density will remain uniform along the portion of the tube occupied by the chain. Uniform compression, however, cannot persist as $z \to 0$ because this would imply a diverging density. At some value of z the chain will develop a hairpin, and the concentration profile along the tube axis will become nonuniform, as illustrated in Figure 1b. There are two possibilities to form a hairpin with a given end position z, as depicted in Figure 1b, and both configurations have the same free energy. The two branches of the free energy, $F_{unif}(z)$, and $F_{hp}(z)$ corresponding to uniform compression and hairpin conformations, respectively, can be determined independently according to standard scaling considerations. By virtue of the mirror symmetry, both branches must be even functions of z.

Assuming a uniform density profile in the portion of the tube occupied by the chain, we write

$$\frac{F_{unif}}{k_BT} = AN\left(\frac{Na^3}{zD^2}\right)^{\alpha} + BN\left(\frac{z}{Na}\right)^{\delta} = A\left(\frac{R^3}{zD^2}\right)^{\alpha} + B\left(\frac{z}{R}\right)^{\delta} \tag{1}$$

where A and B are nonuniversal, model-dependent amplitudes of order unity.

The first term describes the effect of nonbonded volume interactions for semidilute solutions in the form of des Cloizeaux,[44] $F_{conc}/k_BT \propto N[a^3\phi]^{1/(3\nu-1)}$, where the segment density is $\phi \propto N/(zD^2)$. Alternatively, one arrives at the same expression in the scaling picture of "concentration blobs" of de Gennes.[45] The correlation length ξ_c of density fluctuations scales with the density ϕ like $\xi_c \propto [a^3\phi]^{\nu/(1-3\nu)}$. Each of these concentration blobs increases the free energy by an amount of the order of the thermal energy, k_BT. Since each concentration blob contains $g_c \propto \phi\xi_c^3 \sim [a^3\phi]^{1/(1-3\nu)}$ segments, the nonbonded interactions contribute to the free energy an amount $k_BT(N/g_c) \propto k_BTN[a^3\phi]^{1/(3\nu-1)}$. Thus, the exponent of the first term in eq 1 is $\alpha = 1/(3\nu - 1)$.

The second term in eq 1 represents the stretching free energy in the Pincus form.[46] The stretched conformation in the uniform state can be conceived as a linear string of tensile blobs of size $\xi_s \propto ag_s^{\nu}$, where g_s denotes the number of segments in a tensile blob. Each tensile blob increases the free energy by an amount k_BT. The end-to-end distance is determined by $z = \xi(N/g_s) = aNg_s^{\nu-1}$. Hence the contribution of chain stretching scales like $k_BTg_s \propto k_BT\,(z/aN)^{1/(1-\nu)}$, i.e., the exponent of the second term in eq 1 is $\delta = 1/(1 - \nu)$.

Minimization of F_{unif} with respect to z yields the equilibrium end-to-end distance

$$l_z^{eq} = \left(\gamma\frac{A}{B}\right)^{\beta} Na(D/a)^{1-(1/\nu)} = \left(\gamma\frac{A}{B}\right)^{\beta} R\left(\frac{D}{R}\right)^{1-(1/\nu)} \tag{2}$$

where $\gamma = ((1 - \nu)/(3\nu - 1))$, $\beta = (((3\nu - 1)(1 - \nu))/(2\nu))$. The equilibrium free energy of confinement is then

$$\frac{F_0}{k_BT} = A^{(3\nu-1)/2\nu}\left(\frac{B}{\gamma}\right)^{(1-\nu)/2\nu}(1 + \gamma)\left(\frac{D}{R}\right)^{-1/\nu} \tag{3}$$

The free energy of the configurations with a hairpin, illustrated in Figure 1b, is obtained from a similar construction:

$$F_{hp}(z|n, y) = nA\left(\frac{na^3}{zD^2}\right)^{\alpha} + nB\left(\frac{z}{na}\right)^{\delta} + (N - n)A$$
$$\left(\frac{(N - n)a^3}{yD^2}\right)^{\alpha} + (N - n)B\left(\frac{2y}{(N - n)a}\right)^{\delta} \tag{4}$$

dx.doi.org/10.1021/ma500053n | Macromolecules XXXX, XXX, XXX–XXX

where the first two terms refer to the single-strand part of the chain, containing n segments within an end-to-end distance z, whereas the last two terms describe a hairpin of length y, comprised of two strands of $(N - n)/2$ segments each. The two extra variables, y and n, are subject to optimization. The result of this minimization has the meaning of a nonequilibrium Landau free energy controlling the probability density of the end coordinate, z. A closed-form analytical solution is available. The fraction of segments in the single-strand part is

$$\frac{n}{N} = \begin{cases} \dfrac{z}{Z^*}, & |z| \le Z^* \\ 1, & |z| > Z^* \end{cases} \tag{5}$$

where $Z^* = ql_z^{eq}$ is a fraction of the equilibrium end-to-end distance. The coefficient $q \approx 0.779$ is the root of the transcendental equation $q^{\delta} - 3q^{-\alpha} + 2^{1+(1/3\nu)} = 0$, and is *model-independent* within the scaling approach of eqs 1 − 4. The length of the hairpin, y, is then given by

$$y = 2^{(1-3\nu)/2\nu}\left(\frac{A\gamma}{B}\right)^{\beta}(N - n)D^{1-1/\nu} \tag{6}$$

Taking into account eq 5, this result can be written in a model-independent form,

$$\frac{y}{l_z^{eq}} = 2^{(1-3\nu)/2\nu}\left(1 - \frac{|z|}{ql_z^{eq}}\right) \tag{7}$$

It is clear from eq 6, that a hairpin starts to develop at $z = Z^*$ and continuously grows with the decrease in z, resembling a second-order transition. The theory suggests that, for a perfectly flexible chain, *no* activation barrier is involved in the hairpin formation. Note, however, that the scaling description used above is not expected to be accurate, if either the hairpin or the single strand contains one blob or less.

As a result, both branches of the Landau free energy can be combined together, see Figure 2. In reduced variables,

$$\frac{F(z)}{F_0} = \begin{cases} 2^{1/2\nu} - p\dfrac{|z|}{l_z^{eq}}, & |z| \le Z^* \\ \dfrac{1}{\gamma + 1}\left(\dfrac{|z|}{l_z^{eq}}\right)^{-\gamma} + \dfrac{\gamma}{\gamma + 1}\left(\dfrac{|z|}{l_z^{eq}}\right)^{\delta}, & |z| > Z^* \end{cases} \tag{8}$$

Here we express the Landau free energy, $F(z)$, in terms of the equilibrium free energy of confinement, eq 3, and the coordinate, z, of the free end, using the equilibrium end-to-end distance, eq 2. The slope $p = 2^{1/2\nu}q^{-1} - (1/(1 + \gamma))\, q^{-1-\alpha} - (\gamma/(1 + \gamma))\, \alpha^{\delta-1}$ is model-*independent* within the scaling approach, and adopts the numerical value $p \approx 0.91$.

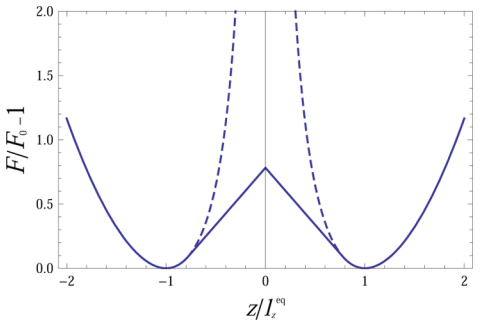

Figure 2. Landau free energy, $F(z)$ cf. eq 8, normalized by the equilibrium value as a function of the end coordinate, z. The dotted line describes a strictly uniform deformation, F_{unif} cf. eq 1. The two curves start to deviate at about $Z^*/l_z^{eq} = 0.779$.

Obviously, the free energy of a configuration with a hairpin does not depend on the loop position (right or left), see Figure 1b. Moreover, within the scaling approach of eq 4 the free energy would be exactly the same, if there simultaneously were two loops (on the right and on the left) of lengths y_r, and $y_l = y - y_r$, respectively, provided their total length, y, were still given by eq 7. This multiplicity of conformations differing by the length of the right loop, y_r, gives rise to logarithmic corrections to the Landau free energy. Asymptotically, these corrections are negligible but for relatively short chains appearing in the current simulations we attempt to give a semiquantitative estimate. The total statistical weight must be associated with an integral over different right/left hairpin lengths, $W(z) = \int_0^y dy_r \exp[-F(z)]$. However, this continuum of conformations must be compared with a single conformation in the absence of hairpins which brings the question of how large must a difference in y_r be so as to qualify as a distinct new conformation. The problem is rooted in the nature of the theoretical description based on the free energy minimization procedure. Effectively, the statistical weight of a single conformation includes some fluctuations on the blob scale. This suggests that the integration variable, y_r, must be properly scaled by the blob size, D. Moreover, a single-conformation contribution must survive even if the range of integration, y, shrinks to zero. Thus, a tentative way of accounting for multiple hairpin conformations is

$$\begin{aligned} W(z) &\approx e^{-F(z)} + \frac{1}{D}\int_0^y dy_r\, e^{-F(z)} \\ &= e^{-F(z)}\left[1 + 2^{(1-3\nu)/2\nu}\frac{l_z^{eq}}{D}\left(1 + \frac{|z|}{ql_z^{eq}}\right)\right], \quad |z| \le q \end{aligned} \tag{9}$$

A numerical factor of order unity may appear with the integral reflecting some arbitrariness in the blob definition.

Finding the distribution function for the center-of mass coordinate is more involved. For each end coordinate, z, the mapping between z and the center-of-mass coordinate, z_{cm}, depends on the type of conformation. For a uniform conformation, $|z| > Z^*$, one has

$$z_{cm} = z/2 \tag{10}$$

For conformations with a hairpin one obtains

$$z_{cm} = \begin{cases} -\dfrac{2^{(1-3\nu)/2\nu}l_z^{eq}}{2}\left(1 - \dfrac{z}{l_z^{eq}}\right)^2 + \dfrac{l_z^{eq}}{2q}\left(\dfrac{z}{l_z^{eq}}\right)^2 \\ \quad + y_r\left[1 + \dfrac{z}{l_z^{eq}}\left(\dfrac{1}{2^{(1-3\nu)/2\nu}} - \dfrac{1}{q}\right)\right], \quad z \ge 0 \\ -\dfrac{2^{(1-3\nu)/2\nu}l_z^{eq}}{2}\left(1 + \dfrac{z}{l_z^{eq}}\right)^2 + \dfrac{l_z^{eq}}{2q}\left(\dfrac{z}{l_z^{eq}}\right)^2 + z \\ \quad + y_r\left[1 - \dfrac{z}{l_z^{eq}}\left(\dfrac{1}{2^{(1-3\nu)/2\nu}} - \dfrac{1}{q}\right)\right], \quad z \le 0 \end{cases} \tag{11}$$

where y_r is the length of the right loop. Mapping between z and z_{cm} involves one, (eq 10), or multiple, (eq 11), branches, depending on whether hairpins are involved. Figure 3 shows

dx.doi.org/10.1021/ma500053n | Macromolecules XXXX, XXX, XXX−XXX

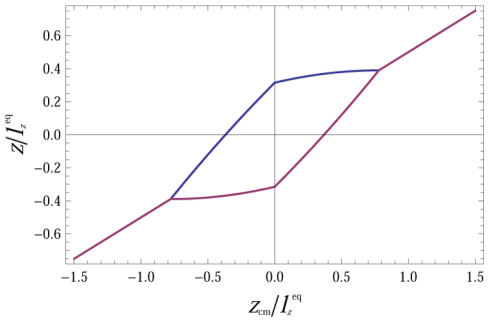

Figure 3. End position expressed in terms of the center-of-mass coordinate, z_{cm}.

the boundary of the multivalued mapping region. The branching point corresponds to $z = Z^*$, $z_{cm} = Z^*/2$ while the center-of-mass position at the origin, $z_{cm} = 0$, can be achieved with the free end coordinate in the range $(|z|/l_z^{eq}) \leq (q2^{(1-3\nu)/4\nu})/(\sqrt{q} + 2^{(1-3\nu)/4\nu}) \approx 0.37$.

In the spirit of eq 9, the total statistical weight, associated with a given value of z_{cm}, is expressed as

$$W(z_{cm}) = \begin{cases} \exp\{-F_{min}[z(z_{cm}, y_r)]\} + \frac{1}{D}\int_0^y dy_r \exp\{F[z(z_{cm}, y_r)]\}, \\ \quad |z_{cm}| \leq \frac{Z^*}{2} \\ \exp\{-F[2z_{cm}]\}, \quad |z_{cm}| > \frac{Z^*}{2} \end{cases} \tag{12}$$

where the function $z(z_{cm},y_r)$ is obtained by inverting eqs 11 and $\exp\{-F_{min}[z(z_{cm},y_r)]\}$ is the dominant contribution due to the lowest free energy conformation for a given z_{cm}. Logarithmic plots of the probability densities for the end position, z, and the center-of-mass coordinate, z_{cm}, are displayed in Figure 4 for $D/a = 4$, $N = 25$, i.e., $D/R \approx 0.6$. The values of the constants $A = 0.65$, $B = 1.95$ were taken from fitting the Monte Carlo data for a lattice chain in tube,[47] but the shape of the curves is not very sensitive to these values.[48]

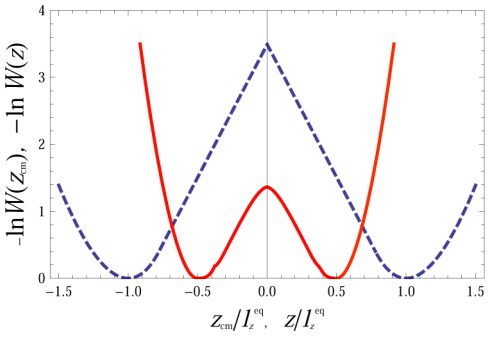

Figure 4. Landau free energy for the center-of-mass coordinate, z_{cm} (solid line), in comparison with that for the chain end position, z (dashed line). $N = 25$, $D = 4a$.

The behavior of $W(z_{cm})$ near $z = \pm Z^*/2$ was smoothed by allowing for some pretransitional increase in fluctuations to avoid jumps at the bifurcation points of Figure 3. For asymptotically long chains the barrier heights differ approximately by a factor of 1.7. For the center of mass at the origin, it is enough to bring the free end within a distance of $0.37l_z^{eq}$.

Both distributions are symmetric and bistable, with the equilibrium position of the center of mass being approximately one-half of the end position. However, the heights in the maxima differ quite dramatically. The maximum of $W(z)$ occurs at $z = 0$, i.e., the free end moves from one side of the tethering point to the other. Within the framework of the scaling consideration, this conformation provides an approximation for the saddle point of the transition path and $W_{max} = W(z = 0)$ provides an estimate for the free-energy barrier.

The maximum of $W(z_{cm})$ is significantly smaller because at $z_{cm} = 0$ half of the molecules have a left bend and the other half have a right bend yet the free chain end is not at $z = 0$ (see Figure 1) but rather at $z = \pm l_z^{eq}$, according to Figure 3. In fact, changing the position of the center of mass from positive to negative values (with respect to the tethered end) does not require complete arm retraction and flipping. Therefore, we conclude that z_{cm} is not a good reaction coordinate to describe the progression of the transition of the free chain end from one side to the other side of the tethering point, and the maximum of $W(z_{cm})$ cannot be interpreted as a barrier height that controls the arm retraction dynamics.

B. Two Tethered Chains in a Tube. Another example of a bistable equilibrium appears in a star polymer confined in a tube and refers to the conformation of two grafted branches sharing the same orientation as sketched in Figure 5a. In fact, this case is identical to dealing with a pair of chains, end-tethered to the bottom of a capped nanopore, cf. Figure 5b, which we shall consider below too.

Although the two chains have the same contour length, the distance of their ends from the tethering point turns out to be different in equilibrium, demonstrating a curious example of spontaneous symmetry breaking. In order to demonstrate this more clearly, we construct the free energy, $F(z_1,z_2)$, as a function of the two end-coordinates, z_1 and z_2, which defines the joint probability density of the end-to-end distance distribution. The starting expression is constructed along the same line as eqs 5 and 10:

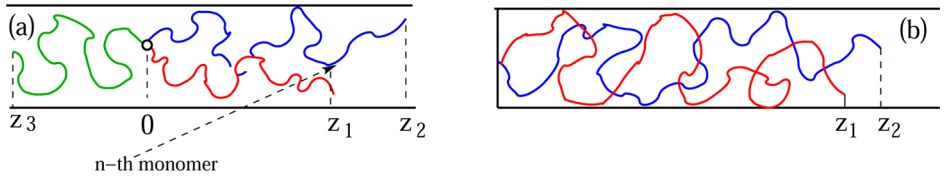

Figure 5. (a) Three-arm star in a narrow tube: The two arms with the same orientation generally have different equilibrium end-to-end distances z_1, z_2, which are also different from that of a single arm with the opposite orientation, $z_3 = l_z^{eq}$. The arm with the strongest stretching has n monomers in the strand within the range $(0, z_1)$ and $N - n$ monomers beyond z_1. (b) Bistable system of a pair of confined chains tethered to the bottom of capped nanopore.

dx.doi.org/10.1021/ma500053n | Macromolecules XXXX, XXX, XXX−XXX

$$F(z_1, z_2|n) = (N+n)A\left(\frac{(N+n)a^3}{z_1 D^2}\right)^{\alpha} + BN\left(\frac{z_1}{Na}\right)^{\delta} + Bn\left(\frac{z_1}{na}\right)^{\delta} + (N-n)A\left(\frac{(N-n)a^3}{(z_2-z_1)D^2}\right)^{\alpha} + (N-n)B\left(\frac{z_2-z_1}{(N-n)a}\right)^{\delta} \quad (13)$$

Here n is the number of monomers in the second arm, $z_2 > z_1$, which share the space with all N segments of the first branch within the range $(0, z_1)$ of the tube. The first three terms describe the concentration and the elastic free energy of two strands within this tube section, whereas the last two terms refer to the end section of the second arm, containing $N - n$ monomers. The variable n is subject to minimization at fixed z_1 and z_2. In contrast to the problem of hairpin formation, there is no analytical solution in this case. The free energy landscape, $F(z_1, z_2)$, obtained by numerical minimization, is shown in Figure 6. The chain-end coordinates and the free energy itself are scaled by l_z^{eq} and F_0, respectively, see eqs 2 and 3. The graph clearly shows two minima at ($\langle z_1\rangle \approx 0.951 l_z^{eq}, \langle z_2\rangle \approx 1.4 l_z^{eq}$) and the symmetry-related pair.

The distribution density for the end-separation, $W(z_2 - z_1)$, is obtained from $F(z_1, z_2)$ by integrating over the center-of-mass coordinate:

$$W(z_2 - z_1) = \int_{|z_2-z_1|/2}^{\infty} \exp\left(-F\left[y - \frac{z_2 - z_1}{2}, y + \frac{z_2 - z_1}{2}\right]\right) dy \quad (14)$$

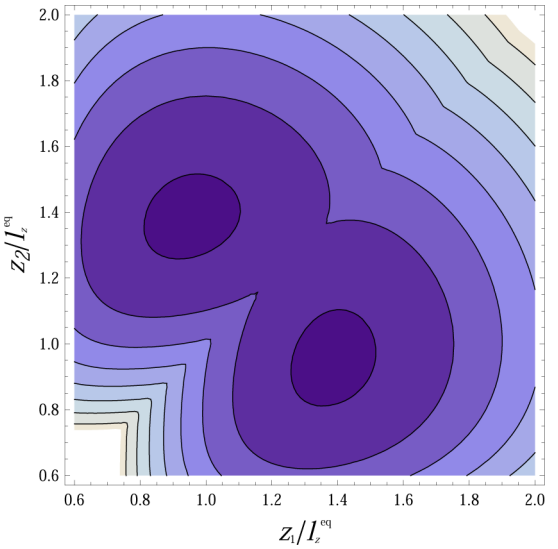

Figure 6. Contour plot of the free energy landscape $F(z_1,z_2)$.

III. COMPUTER SIMULATIONS: MODEL AND TECHNIQUES

A. Molecular Dynamics Simulation of a Star Polymer in a Pore. We consider a three-dimensional coarse-grained model[20] of a star polymer that consists of $f = 3$ linear arms. One end of each arm is free whereas the other one is tethered to a microscopic core- (or junction)-monomer of size σ_{core}, which is of the size of a monomer σ, cf. Figure 7. Each arm is comprised of N particles of equal size and mass, connected by finitely −extensible elastic bonds. Thus, the total number of monomers in the star (excluding the core) is fN.

The nonbonded interactions between all monomers are taken into account by means of the Weeks−Chandler−Andersen (WCA) interaction, i.e., by the shifted and truncated repulsive branch of the Lennard-Jones potential:

$$V^{WCA}(r) = 4\varepsilon[(\sigma/r)^{12} - (\sigma/r)^6 + 1/4], \text{ for } r < 2^{1/6}\sigma \quad (15)$$

and 0 for larger distances, r. These interactions mimic steric repulsion typical for polymers under good solvent conditions. Additionally, bonded beads are connected by the "finitely extensible nonlinear elastic" (FENE) potential:[26]

$$V^{FENE}(r) = -0.5kr_0^2 \ln[1 - (r/r_0)^2] \quad (16)$$

In eqs 15 and 16, r denotes the distance between the centers of two segments (beads), while the energy scale ε and the length scale σ are chosen as the units of energy and length, respectively. Accordingly, the remaining parameters are fixed at the values $k = 30\varepsilon/\sigma^2$ and $r_0 = 1.5$. The confining tube is

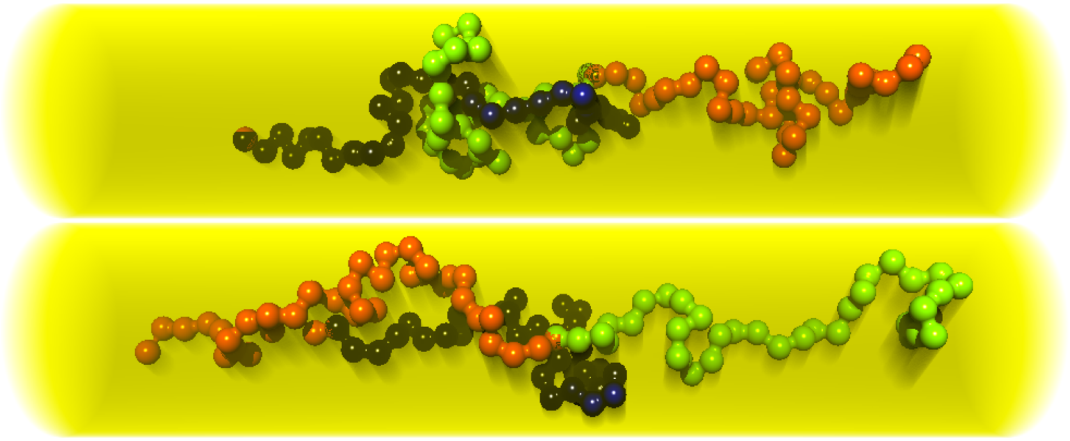

Figure 7. Snapshots of a star polymer with $f = 3$ arms of length $N = 35$ in a tube with $\kappa = 0.1$ before (upper panel), and after (lower panel) 10^7 integration steps have been performed. The second configuration corresponds to an partially "activated state" of the black chain, associated with a free energy barrier. During the time interval between the two snapshots, the red and the green arms have swapped positions in the tube.

dx.doi.org/10.1021/ma500053n | Macromolecules XXXX, XXX, XXX−XXX

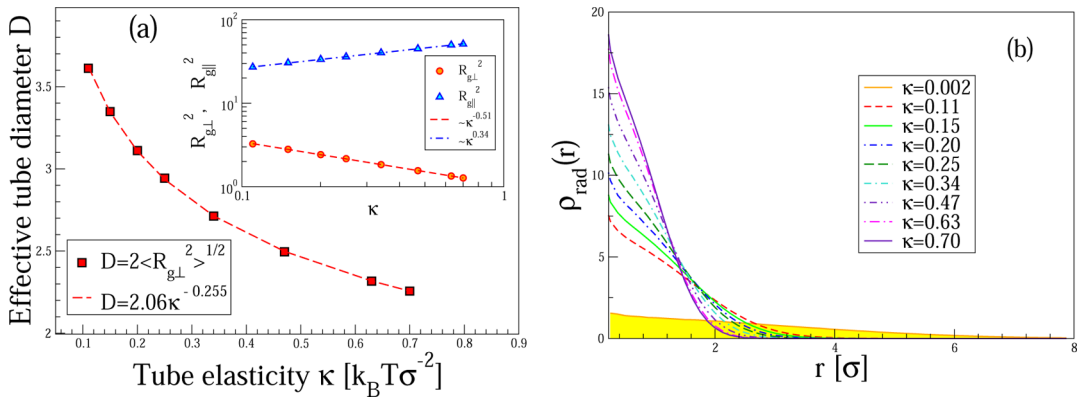

Figure 8. (a) Effective tube diameter D vs parameter κ from eq 17. Inset: Variation of gyration radius components $R_{g\perp}{}^2$ and $R_{g\parallel}{}^2$ perpendicular and parallel to tube axis with elasticity constant κ for a star polymer with $f = 3$ and $N = 25$. (b) Radial density distribution $\rho_{rad}(r)$ of monomers for different values of κ.

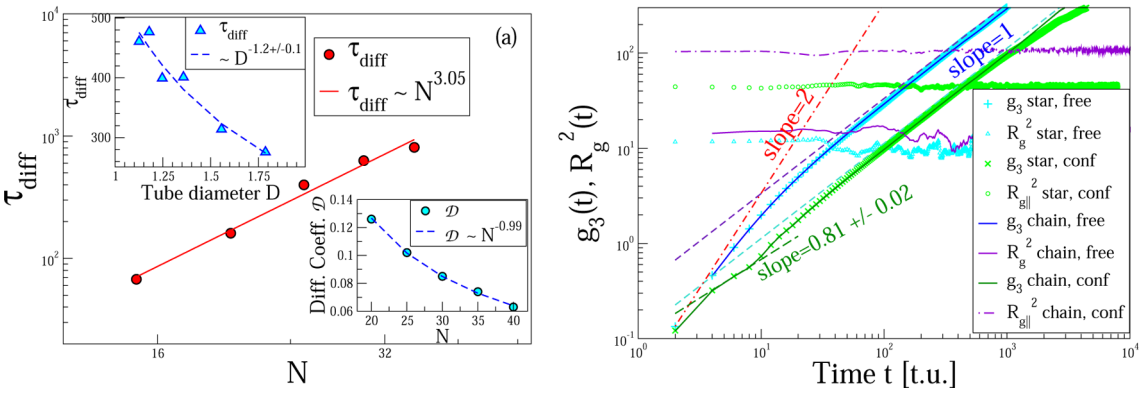

Figure 9. (a) Variation of the characteristic relaxation time, $\tau_{diff} \propto N^3$, of a three-arm star-polymer with arm length N at constant tube diameter, D, corresponding to $\kappa = 0.1$. In the inset (left) we verify another result, $\tau_{diff} \propto D^{2-2/\nu} \approx D^{-4/3}$, in the inset (right), the diffusion coefficient $\mathcal{D} \propto N^{-0.99\pm0.02}$, in agreement with scaling predictions. (b) Center-of-mass MSQD $g_3(t)$ for a star polymer with $f = 3$,$N = 25$, and for a linear chain with the same mass (i.e., with length $N_{tot} = 76$). Here the measured diffusion coefficient $\mathcal{D} = 0.051 \pm 0.002$. For both macromolecules $g_3(t)$ coincide irrespective of existing confinement. In the nanopore, one observes a confinement-induced anomalous diffusion in a narrow interval with $g_3(t) \propto t^{0.81}$. Nonetheless, the relaxation time τ_{diff} for diffusion of the linear chain is about 75% larger than that of the star because of chain's larger $R_{g,z}{}^2$.

modeled as a cylindrical potential with *soft* walls,[49] imposed by a harmonic potential around the z-axis:

$$V^{tube}(r) = -\kappa(r_x{}^2 + r_y{}^2) \tag{17}$$

and characterized by an elastic constant κ, that determines the effective diameter, D, of the tube, as demonstrated in Figure 8a. We define the effective tube diameter D as twice the measured radius of gyration of the star polymer, $D = 2R_{g\perp}$, perpendicular to the tube axis for each given value of κ. Thus, we assume the tube to be a cylinder of circular cross-section. Such a potential is appropriate for pores and channels in soft, flexible matrix materials, but this softness of the confinement does not alter the qualitative behavior of the star-polymer in the present study.

The equilibrium dynamics of the chains is obtained by solving the Langevin equation of motion for the position $\mathbf{r}_n = [x_n, y_n, z_n]$ of each bead of the star polymer,

$$m\ddot{\mathbf{r}}_n = \mathbf{F}_n^{FENE} + \mathbf{F}_n^{WCA} - \gamma\dot{\mathbf{r}}_n + \mathbf{R}_n(t), \quad n = 1, ..., fN \tag{18}$$

which describes the Brownian motion of a set of interacting monomers.

In eq 18 above, $\mathbf{F}_n^{FENE}$ and $\mathbf{F}_n^{WCA}$ are the deterministic forces exerted on monomer n by the neighboring bonded and nonbonded monomers, respectively. The influence of the solvent is split into a slowly evolving friction force $-\gamma\dot{r}_n$ and a rapidly fluctuating stochastic force. This random, Gaussian force $\mathbf{R}_n$ is related to friction coefficient γ via the fluctuation–dissipation theorem. We employ an integration steps $\Delta t = 0.002\tau_{MD}$, where time is measured in units of $\tau_{MD} = (m\sigma^2/\varepsilon)^{1/2}$; $m = 1$ denoting the mass of the beads. We integrate the equations of motion, eq 18, employing the velocity–Verlet algorithm.

Starting configurations were generated as straight chains, placed inside the tube parallel to the z-axis, and equilibrated for about $10^5{}_{\tau_{MD}}$ in the field, eq 17, before production runs were carried out.

As one may verify from Figure 8a, there exists a simple effective relationship, $R_{g\perp}{}^2 = 1.06\kappa^{-0.51}$, between the perpendicular size of the star polymer and the elastic constant of the tube, κ. According to the scaling considerations of section II, the free energy of a chain inside the soft tube scales like $F_{tube}(D) = ak_BT(R/D)^\delta + b\kappa ND^2$ with constants, a and b, of order unity. The first term describes the entropy loss due to stretching, cf. eq 1, whereas the second term quantifies the energy in the confining field. Minimization with respect to D yields the scaling prediction $D \propto ((k_BT/\kappa N)R)^{1/\delta+2} =$

dx.doi.org/10.1021/ma500053n | Macromolecules XXXX, XXX, XXX–XXX

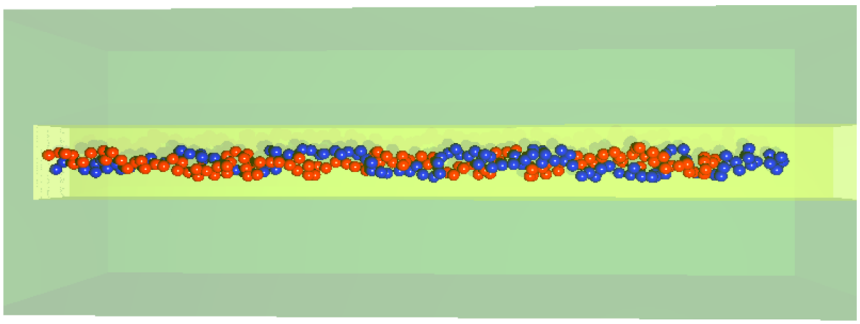

Figure 10. Snapshots of two polymer chains, each of length $N = 128$, tethered to the bottom of a channel with $D \times D$ rectangular cross-section (here $D = 2$). The end-monomer positions of the chains, z_1 and z_2, differ and alternate in time.

$((k_BTa^{\delta}N^{\nu/1-\nu})/\kappa)^{1/\delta+2}$, where $1/(\delta + 2) = ((1 - \nu)/(3 - 2\nu)) \approx 0.226$.

The observed relation $D = 2R_{g\perp} \propto \kappa^{-0.255}$ corroborates this phenomenological consideration. The mean squared end-to-end distance between the core-monomer and the arm-end monomers, and the radius of gyration along the tube, scale like ${R_{arm}}^2 \propto {R_{g\|}}^2 = 58.2\kappa^{0.345}$. Using the observed relation between the effective tube diameter D and the strength of the confining field, $\kappa \propto D^{1/(0.255\pm0.002)}$, one obtains $R_{g\|} \propto D^{-0.676\pm0.005}$, which is a nice confirmation of the expected polymer size dependence, $\propto D^{1-1/\nu}$, under cylindrical constraints.

In Figure 8b we show also the variation of the radial monomer density $\rho_{rad}(r)$, perpendicular to the tube axis, for different values of κ, demonstrating that for $\kappa > 0.2$ the tube walls act as a well-defined constraint even for comparatively short arms.

Additionally, we have monitored the effect of soft, cylindrical confinement on the star polymer dynamics. In Figure 9 we show the total (three-dimensional) mean-squared displacement (MSQD) of the star polymer center-of-mass, $g_3(t) = \langle[r_{cm}(t) - r_{cm}(0)]^2\rangle$. At long times, the diffusion of the center-of-mass position is along the tube and we observe a Rouse-like scaling of the diffusion constant, $\mathcal{D} = \lim_{t\to\infty} (g_3(t))/(6t)$ with the inverse chain length, $D \propto 1/N$. From these data we define a characteristic diffusion time according to $g_3(\tau_{diff}) = {R_{g\|}}^2$, i.e., τ_{diff} is the time that it takes the confined star polymer to diffuse a distance of its own size in the tube. The previous scaling analysis suggests ${R_{g\|}}^2 \propto (l_z^{eq})^2 \propto N^2D^{2-2/\nu}$, yielding $\tau_{diff} \propto D^{2-2/\nu}N^3$.[50] Figure 9a then presents the variation of the characteristic diffusion time, τ_{diff}, as a function of the arm length N and the effective tube diameter D, demonstrating good agreement with these scaling predictions, even though we test these predictions for rather small tube diameters, D, and short chain lengths, N, where corrections to scaling might be expected.

It is of some interest to compare the confined dynamics of a star polymer in a cylindrical tube to that of a linear polymer chain with the *same* molecular weight, cf. Figure 9b. Evidently, the topological difference of both macromolecules has virtually no effect on the MSQD $g_{3\|}$ along the tube, irrespective of whether geometric constraints are present or not; i.e., $g_{3\|}$ is virtually identical for linear chains and stars, with or without confinement. This behavior is expected, according to the Rouse model where in all four cases no force acts along the tube axis. The MSQD perpendicular to the tube axis, $g_{3\perp}$, however, differ. At very early times, the center-of-mass does not "feel" the geometric confinement and the diffusive displacement is isotropic. After a short time interval, $t_{cross} \propto D^2/\mathcal{D}$, however, the forces that the confining potential exerts on the center of mass limit the increase of $g_{3\perp}$, and it attains a finite asymptotic value that is proportional to D^2. Since the local density of a linear chain is smaller than that of a star,[51] the same value of κ results in an effectively larger $D \propto R_{g\perp}$ for the linear chain, and the asymptotic value of $g_{3\perp}$ becomes larger for linear chains than star polymers.

B. Monte Carlo Simulation of a Pair of Chains Tethered to the Bottom of a Nanopore. Another example, similar to the bistable behavior of star arms in confinement, is the case of two linear polymer chains in a nanopore. We investigate the behavior of two polymer chains, tethered to the bottom of a narrow channel, in a hard capped tube, demonstrating that there is no qualitative difference between hard and soft confinement for the properties that we study. The use of both MD and Monte Carlo methods should also make certain that no artifacts, pertinent to a particular simulation model, may be associated with our observations.

The Monte Carlo simulations use a well-established coarse-grained off-lattice bead–spring model.[52−55] The "springs" that connect bonded segments are described by a finitely extensible nonlinear elastic FENE potential for both star polymers and linear chains

$$U_{FENE}(l) = U_0 \ln\left[1 - \left(\frac{l - l_0}{l_0 - l_{max}}\right)^2\right] \tag{19}$$

where l is the length of a bond connecting two neighboring segments, which can vary between $l_{max}(\equiv 1$, chosen as our unit of length) and $l_{min}(=0.4)$, with a potential minimum at $l_0 = 0.7$, halfway in between the minimum and the maximum bond extension. The amplitude U_0 of this potential is chosen as $U_0 = 20$, using the thermal energy $k_BT = 1$ as our energy unit.

The nonbonded interactions between any pair of segments are described by the Morse potential,

$$U_M(r)/\varepsilon = \exp[-2\alpha(r - r_{min})] - 2\exp[-\alpha(r - r_{min})] \tag{20}$$

which has a minimum at $r_{min} = 0.8$. The minimum is rather sharp because we use a large value of the parameter $\alpha = 24$,[52−55] implying that the range of this attraction is always very short, so it can be truncated at $r = 1$, which is useful to make the algorithm efficient and fast.

The pore is modeled as a capped rectangular prism of thickness D and pore length that exceeds the contour length of the polymer chains, cf. Figure 10. The walls of the pore are impenetrable for the chain segments. Both chains are tethered with their first segment to the bottom of the pore and during

dx.doi.org/10.1021/ma500053n | *Macromolecules* XXXX, XXX, XXX−XXX

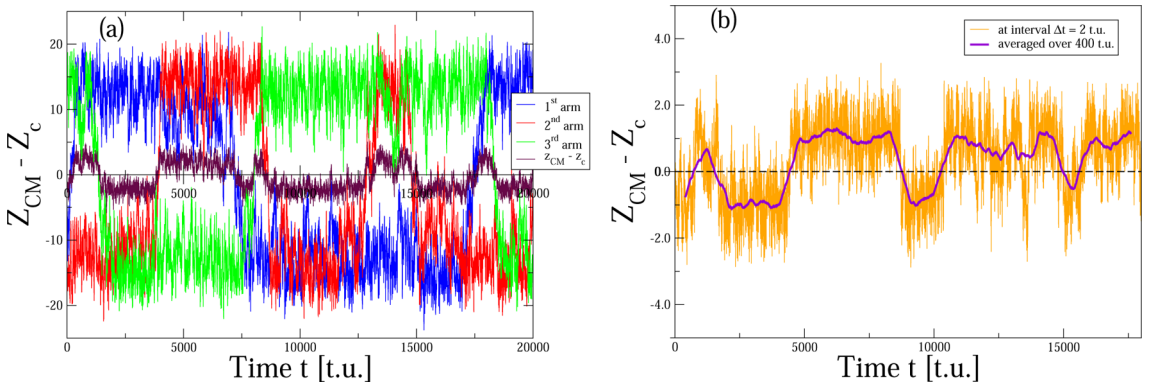

Figure 11. Arm retraction dynamics of a star polymer with $f = 3$ and $N = 35$ in a soft tube with $D \approx 3.11$, corresponding to $\kappa = 0.20$. The time-dependent end-monomer positions of the arms with respect to the position, $z_c(t)$ of the core segment, are marked by different colors. The center-of-mass position $z_{cm}(t)$ with respect to $z_c(t)$ is shown by thick black line. (b) Center-of-mass fluctuations $z_{cm}(t)$ around z_c (thin line) and a running average over $200\tau_{MD}$ of the same data (thick line) for $f = 3$, $N = 25$ and $D = 2.5$.

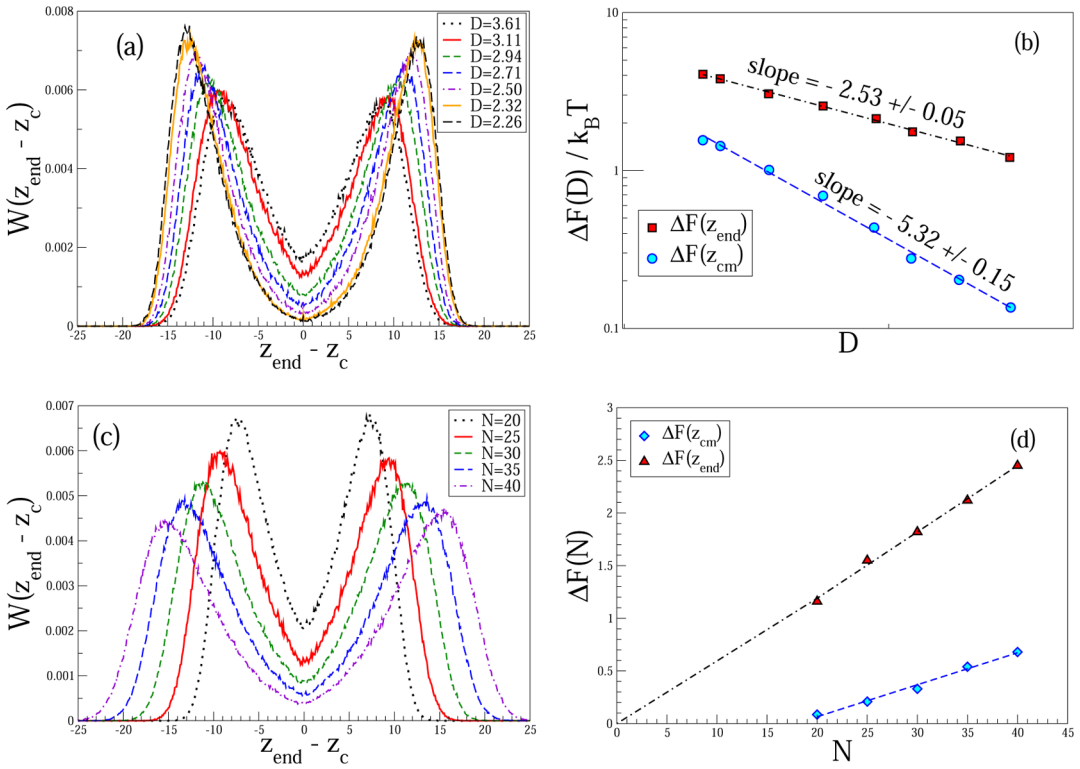

Figure 12. (a) Probability distribution $W(z_{end} - z_c)$ of the position z_{end} of a free end for different tube diameters D. (b) Maximum of the Landau free energy vs D for flipping chain ends, $\Delta F(z)$, and for the star center-of-mass, $\Delta F(z_{cm})$ with respect to the core segment, z_c, vs D. The arm length is $N = 25$. (c) Arm end probability distribution, $W(z_{end} - z_c)$, as function of arm length N. (d) $\Delta F(z)$ vs N for a tube with $D = 3.35$. One finds $\Delta F/k_BT \propto D^{-2.5}$ for the end-monomers of the arms, and a linear variation of ΔF with N.

the simulation we monitor the positions of the free end-segments, z_1 and z_2.

The Monte Carlo algorithm consists of attempted moves, whereby a monomer is chosen at random and one attempts to displace it to a new randomly chosen position with displacements Δx, Δy, Δz, drawn from the intervals $-0.5 \leq \Delta x, \Delta y, \Delta z \leq +0.5$. These trial moves are accepted or rejected according to the standard Metropolis test.[56]

IV. SIMULATION RESULTS

A. Arm Retraction Dynamics of a Confined Star Polymer. In order to illustrate the arm retraction dynamics of a single star polymer in a narrow tube, we first present in Figure 11 the time evolution of the position of the three free end-monomers with respect to the position, z_c, of the star's core-monomer as a function of time, t. One observes that, occasionally, one of arms in the doubly occupied part of the tube threads around the core segment and enters the hitherto low-density part of the tube. After some period of time, one of the arms swaps sides again.

Figure 11a demonstrates that this alternating retraction process correlates with a swapping of the center of mass from one side of the core monomer to the other; i.e., a change of sign of $z_{cm}(t) - z_c(t)$ takes place. A closer inspection of Figure 11b reveals that one observes numerous fluctuations of $z_{cm}(t) - z_c(t)$ around zero for the current set of parameters at maximal

dx.doi.org/10.1021/ma500053n | Macromolecules XXXX, XXX, XXX–XXX

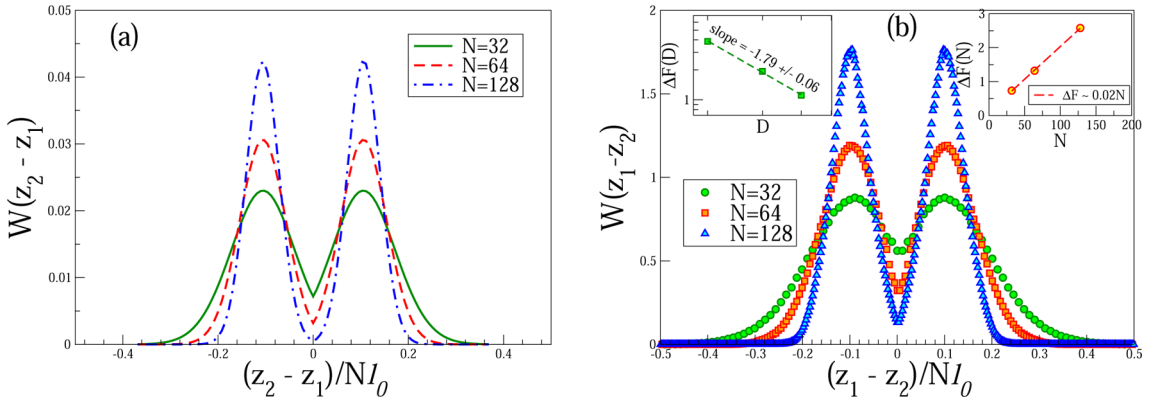

Figure 13. Probability distributions for the difference in end-positions, $z_1 - z_2$, of a pair of confined chains of length N, tethered to the bottom of a narrow tube with diameter $D = 2a$. (a) Theoretical results, according to eq 14. (b) Monte Carlo data. The left inset demonstrates $\Delta F \propto D^{-1.79}$ which is close to expectation, eq 3. The right inset indicates a linear variation of ΔF with the arm length, N, as expected.

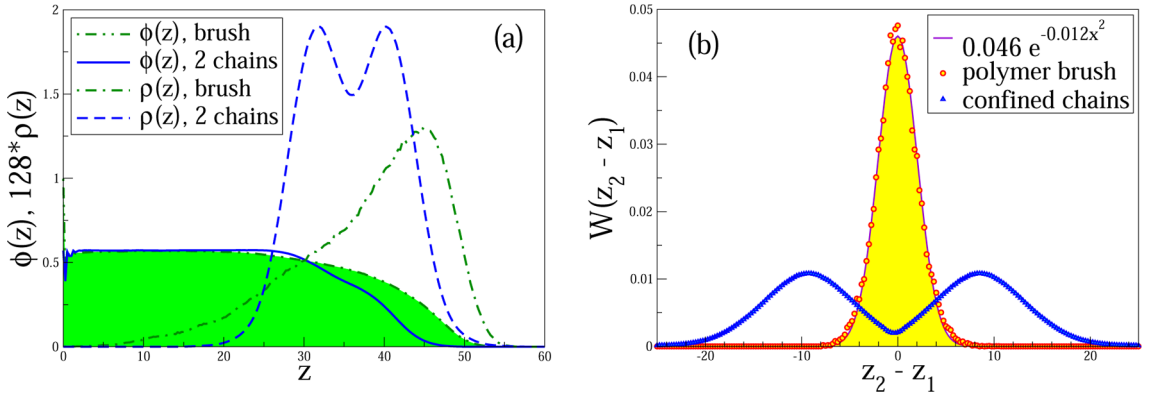

Figure 14. (a) Density profiles of all segment, $\phi(z)$, and the free end segments, $\rho(z)$, of a confined two-chain system and a polymer brush with comparable area densities. (b) Probability distribution of the difference $x = z_2 - z_1$ of end-segment positions for the same systems as in panel a.

resolution of time events. These rapid changes between positive and negative values of $z_{cm}(t) - z_c(t)$, however, do not reflect the life times of equilibrium star-polymer configurations. In accord with the consideration in section II, they originate from short-lived transient conformations when the center of mass, z_{cm}, briefly changes place with the core monomer, z_c, and then immediately goes back again. Since $z_{cm}(t) - z_c(t)$ may change sign when an arm end only partially threads beyond z_c without reaching the new equilibrium distance on the other side, these sign changes do not signal real crossing of the barrier along the transition path of an arm switching sides.

In contrast, comparatively lengthy periods of sustained configurations are seen to persist, if a running average of the rapid fluctuations over, e.g., 20 to 200 time units, cf. Figure 11b, is carried out. Evidently, the center-of-mass switches sides more frequently than the monomers at arm ends, so the latter appear more appropriate to be taken as a reaction coordinate of the retraction process. This change of end position requires crossing of an energy barrier ΔF, separating the two stable conformations with two arms on the one side of z_c, and the third arm residing on the opposite side of z_c.

In Figure 12a, we show the measured probability distribution $W(z - z_c)$ of arm ends (with respect to the star's core position, z_c), for pores with different diameter D. From these measurements, one can obtain the free energy profile as $F = -k_BT \ln W(z - z_c)$ up to an additive constant, and determine the magnitude of the barrier, ΔF, as a function of D.

The results of such an analysis are presented in Figure 12b. One finds as expected, that $\Delta F(z_{cm}) < \Delta F(z)$, indeed. Moreover, the power-law relationship $\Delta F \propto D^{-\eta}$ exhibits different exponents $\eta \approx 2.53 \pm 0.05$ and $\eta \approx 5.32 \pm 0.15$ for arm ends and center of mass of the star polymer, which markedly differ from the expected $\Delta F \propto D^{-1/\nu} \sim D^{-1.70}$ behavior, cf. Equation 3. In any case, the free-energy barrier for z_{cm} deviates more from the expected value than that for the arm ends, where the barrier height exceeds k_BT. Moreover, the range of variation of the tube diameter, D, is rather narrow and, therefore, certainly far from the asymptotic scaling regime. Figure 12d clearly shows the correct linear variation of the barrier with arm length N (the extrapolated straight line goes through zero) for the arm ends. For the center of mass, as mentioned, the magnitude of the barrier is only of the order of k_BT for the chosen chain lengths, N, which are evidently too short for observing the expected asymptotic large-N scaling behavior.

B. Two End-Tethered Chains in a Nanotube: Distribution of Chain Ends. We have checked the analytical expression, eq 8, for the simple case of a soft bistable system: a pair of confined polymers, end-tethered to the capped bottom of a nanopore, cf. Figure 5b and Figure 10. Theoretical curves for $D = 4$, $N = 32$, 64, 128 are shown in Figure 13a, where also a comparison with data, derived from a Monte Carlo simulation of the same system, are presented, cf. Figure 13b, in very good agreement with the theoretical predictions.

dx.doi.org/10.1021/ma500053n | Macromolecules XXXX, XXX, XXX–XXX

The segregation of the end positions becomes more pronounced with the increase in the arm lengths, and this trend is supported by simulation data—cf. Figure 13a,b. The scaling theory slightly overestimates the spatial separation $(\langle(z_2 - z_1)^2\rangle)^{1/2}$.

It is also of interest to compare the behavior of two chains end-tethered in a tube to that of a polymer brush. Indeed, blob arguments similar to those in section II have also been applied to brushes.[57−59] Since the brush is in a good solvent, the excluded-volume interaction is strong,[60] and the chain statistics inside the stretching blob is that of a self-avoiding random walk.[57] Under these conditions, the profile is nearly uniform inside the brush and chain ends are enriched at the top of the brush. Figure 14a presents the density profiles of all monomers and free ends for the two-chain system and the brush.

They comply with the theoretical expectation and, moreover, the average density and end-segment profiles of the brush and the two-chain system are very similar. Thus, the geometric confinement of the nanopore exerts a similar pressure as the neighboring chains in a polymer brush, on average.

The nearly uniform density profile inside the brush corresponds to a constant osmotic pressure and allows for large height fluctuations of the chain ends. It has been suggested that these height fluctuations of the chain ends can be exploited to fabricate smart surface coating.[61] In Figure 14b, we compare the relative fluctuations of chain end positions for the two-chain system and the polymer brush using the same parameters that yielded similar average density profiles. We note that the fluctuations of the two systems are qualitatively different. Whereas the probability distribution of the difference of chain-end positions is Gaussian and centered around zero in the brush, the two-chain system exhibits a bimodal distribution. This result indicates that the fluctuations of the two systems are very different; they are much weaker in a brush, where one long flexible polymer interacts with many neighbors and the fluctuations of these interactions average out.[62] In the confined two-chain system no such averaging occurs and a mean-field-like picture of the system yields qualitatively wrong results for fluctuations.

C. Retraction Time Distribution. In Figure 16a we present the retraction time distribution $P(\tau)$ of the arms ends, regarding one of the two free energy minima, that is, τ is determined as the time difference between successive crossings by the end-monomers of the barrier separating the two free energy minima, cf. Figure 15. The theoretical analysis is based on the Fokker-Plank equation for the evolution of the probability density $f(z,t)$ in the presence of a potential of mean force, $F(z) = -k_BT \ln W(z)$:

$$\frac{\partial f}{\partial t} - \frac{\partial}{\partial z}\mathcal{D}\left(\frac{\partial f}{\partial z} + f\frac{\partial F(z)}{\partial z}\right) = 0 \tag{21}$$

It is assumed that the slow dynamic variable, z, can be treated as independent, while the collective effect of the other internal degrees of freedom is manifested in the value of the effective diffusion coefficient, $\mathcal{D}$, and in the shape of the mean force potential, which now has the meaning of a Landau free energy. For the subsequent analysis, we will consider the diffusion coefficient as constant. The equilibrium distribution $f(z)$ is the stationary solution of the Fokker−Planck equation with a natural boundary conditions $f(\pm\infty, t) = 0$. The solution of eq 21 with an initial δ-peak density, $f(z,0) = \delta(z - a)$, an absorbing boundary at $z = b < a$ (to the left of the starting point), and a

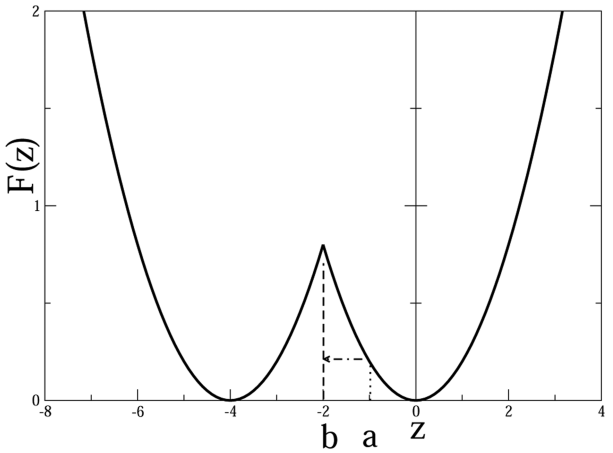

Figure 15. Schematic representation of the first passage time problem in the "double parabolic" approximation.

natural reflecting boundary at at $z \to +\infty$ (to the right of the staring point) generates a distribution of first passage times (FPT) from a to b. Indeed, the integral $\int_b^\infty f(z,t)\,dz$ is the probability to survive within the (b,c) interval by the moment t, and hence, the probability that the first passage time τ from a to b is larger than t. Thus, $\int_b^\infty f(z,t)\,dz = 1 - \mathcal{P}(\tau < t)$, while the first passage time density, $P(\tau)$, is the derivative of the cumulant distribution, $\mathcal{P}(\tau < t)$.

$$P(\tau) = -\frac{\partial}{\partial \tau}\int_b^\infty f(z,\,t)\,dz = \mathcal{D}\frac{\partial f(z,\,\tau)}{\partial z}|z = b \tag{22}$$

where the last equality is obtained by using eq 21 together with the boundary conditions.

An eigenfunction expansion method[63] provides a ready solution

$$f(z,\,t) = \sum_k \alpha_k \varphi_k(z) e^{-\lambda_k t} \tag{23}$$

where the eigenfunctions and eigenvalues are the solutions of the equation

$$-\frac{d}{dz}\mathcal{D}\left[\frac{d}{dz}\varphi_k + \varphi_k\frac{d}{dz}u(z)\right] = \lambda_k\varphi_k \tag{24}$$

satisfying the boundary conditions $\varphi_k(b) = \varphi_k(+\infty) = 0$. The eigenfunctions are orthogonal with an inner product, defined by the weight function $(W(z))^{-1}$, so the coefficients α_k are determined by the initial δ-peak position:

$$\alpha_k = \int_b^\infty f(z,\,0)\varphi_k(z)(W(z))^{-1}\,dz = \frac{\varphi_k(a)}{W(a)} \tag{25}$$

Finally, we obtain the following expression for the FPT distribution:

$$P(\tau) = \sum_k \mathcal{D}\alpha_k\varphi_k'(b)e^{-\lambda_k\tau} \tag{26}$$

In our case, FPT is the time of first crossing the barrier, the absorbing point b can be taken exactly at the barrier top while the starting point a is shifted by distance Δz to the right. The magnitude of Δz is determined by the time discretization scheme (or by the chosen time cutoff in the collected statistics), and is of the order of a typical displacement over one MD time step so that $\Delta z \ll l_z^{eq}$. Taking the complete free energy curve approximately as a combination of two parabolas with a *cusp*

dx.doi.org/10.1021/ma500053n | Macromolecules XXXX, XXX, XXX−XXX

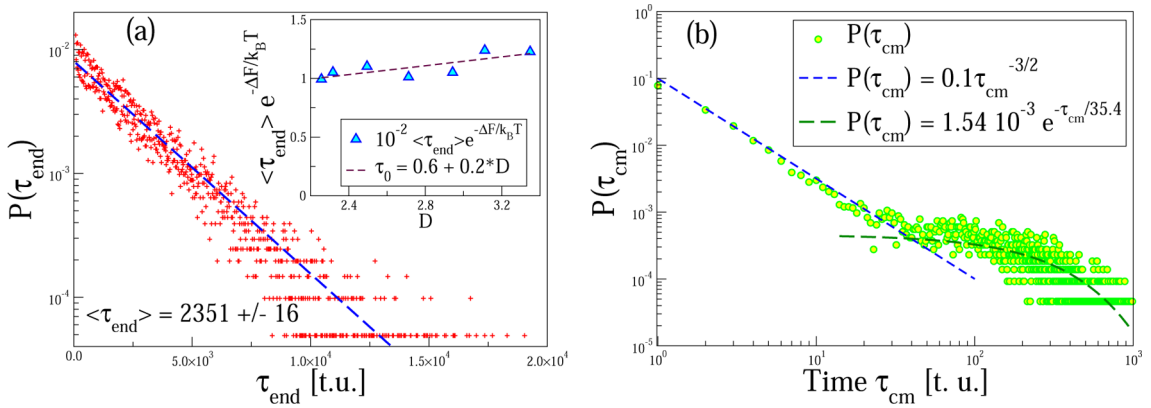

Figure 16. (a) Probability distribution $P(\tau_{end})$ of time intervals between successive transitions of arm ends for $L = 25$, $D = 2.50$. Averaging is performed over 21700 events. The inset shows the attempt rate dependence of the τ_{end} on tube diameter D. (b) Same distribution for the star center-of-mass. At short times $P(\tau_{cm})$ describes fast position exchange with the core monomer position and follows a $\tau_{cm}^{-3/2}$-law, typical for random walk reversals. At longer times $P(\tau_{cm}) \propto \exp(-\tau_{cm}/\langle\tau_{cm}\rangle)$ with $\langle\tau_{cm}\rangle \approx 35.4$.

barrier, Figure 15, the eigenvalue problem admits a solution in terms of Hermite functions:

$$\varphi_k(t) = C_k e^{-k/2z^2} H_k\left(\lambda_k, \sqrt{\frac{k}{2}}z\right) \tag{27}$$

where C_k is a normalization constant, and the right parabola has the form $u(z) = (k/2)z^2$—see Figure 15. The eigenvalues are determined as roots of the equation

$$H\left(\lambda, \sqrt{\frac{k}{2}}b\right) = 0 \tag{28}$$

Here $b < 0$, and $(k/2)^{1/2}b = -(\Delta F)^{1/2}$ with ΔF being the barrier height.

The asymptotic behavior of $P(\tau)$ at small and large τ is easily understood. The initial evolution of the δ-peak is only weakly affected by the gradient of the free energy, and can be taken from a simpler FPT problem in free space:[64]

$$P(\tau) = \frac{\mathcal{D}\Delta z}{\sqrt{\pi}(\mathcal{D}\tau)^{3/2}} \exp\left[-\frac{(\Delta z)^2}{4\mathcal{D}\tau}\right] \tag{29}$$

As far as the diffusion distance Δz is very small, the exponential is close to unity, resulting in a power-law distribution $P(\tau) \propto \tau^{-3/2}$. The long-time τ behavior is dominated by the exponential with the smallest eigenvalue λ_1. The two asymptotic expressions, combined, yield:

$$P(\tau) = \begin{cases} \dfrac{\mathcal{D}\Delta z}{\sqrt{\pi}(\mathcal{D}\tau)^{3/2}}, & \tau\lambda_1 \ll 1 \\ C\exp(-\lambda_1\tau), & \tau\lambda_1 \geq 1 \end{cases} \tag{30}$$

which we find to provide a very good description of the measured $P(\tau)$ in our simulation, see Figure 16.

The mean FPT can be evaluated directly as[65]

$$\langle\tau\rangle = \mathcal{D}^{-1}\int_b^a e^{F(z)}\,dz \int_z^\infty e^{-F(z')}\,dz' \approx \frac{\Delta z}{\mathcal{D}}\sqrt{\frac{2\pi}{F''(z_{min})}}$$
$$\exp(\Delta F) \tag{31}$$

In the last step, we have taken into account that $a - b = \Delta z$ is a small interval of integration, and employed asymptotic integration over z'.

For high enough barriers, $\langle\tau\rangle$ is close to λ^{-1}, extracted from the exponential tail of $P(\tau)$. Since the diffusion coefficient scales as $\mathcal{D} \propto 1/N$, and the free energy curvature at its minimum, is $F''(0) \propto F_0(l_z^{eq})^{-2} \propto N^{-1}D^{1/(\nu-2)}$, the prefactor in the Kramers-type expression, eq 31, is predicted to scale as $N^{3/2}D^{0.15}$. Indeed, the simulation data in Figure 16a at fixed N does show a weak growth of the prefactor as a function of D in good qualitative agreement with the scaling prediction.

In Figure 16a we show our simulation results for $P(\tau_{end})$ for a star polymer with $N = 25$ and tube diameter $D = 2.5$. As expected, one observes an exponential distribution, $P(\tau_{end}) \propto \exp(-\tau_{end}/\langle\tau_{end}\rangle)$, provided one ignores the shortest times when an arm end briefly changes sides with respect to z_c and almost immediately returns to the previous side of the nanopore. If these short times are taken into account, e.g., as in Figure 16b where the residence time distribution for the center of mass, z_{cm}, is plotted, one recovers very clearly the predicted $P(\tau) \propto \tau^{-3/2}$ relationship for $\tau \to 0$, according to eq 16b.

V. CONCLUDING REMARKS

Using molecular dynamics and Monte Carlo simulations and analytical scaling considerations, we have studied the arm-retraction dynamics of a symmetric three-arm star polymer in a narrow nanotube and compared it to the behavior of two chains tethered in an end-capped nanopore. The latter system represents the behavior of the two arms of the star that are on the same side of the star's core. The arm retraction dynamics involves the flipping of one arm from the initially doubly occupied section of the nanopore to the opposite side. This transition involves a free-energy barrier and our results indicate that the distance of the end of the arm from the star's core is an appropriate reaction coordinate. The free-energy barrier increases linearly with chain length, N, and is proportional to $(R/D)^{1/\nu}$ where D and R denote the tube diameter and chain extension in the bulk, respectively. Therefore, the conformational relaxation will become extremely slow for highly confined star polymers. The translational diffusion along the tube, however, is not significantly affected by the confinement. In our model, the diffusion constant exhibits Rouse dynamics $\mathcal{D} \sim 1/N$.

One should note here that the "arm retraction time" in the microscopic stress theory of McLeish-Milner[1] has a somewhat

dx.doi.org/10.1021/ma500053n | Macromolecules XXXX, XXX, XXX–XXX

different connotation from the arm retraction in this work where the confinement effect is due to a persistent soft tube rather than to entanglement-induced *effective* tubes in a melt of star polymers. The basic mechanism of arm retraction, however, is the same. Moreover, it is conceptually similar to the "complete retraction time" reported in some "slip-link models" by Masubuchi et al.[66,67] and others[68] in branched polymer dynamics.

In analogy to a polymer brush, scaling considerations conceive the confined star as a linear string of blobs along the nanopore axis. Therefore, the density inside the tube is nearly uniform and the star extension along the pore scales like $R_{\|} \sim N$. In accord with the scaling picture and with the behavior of a polymer brush too, we observe in the simulations that the free ends of the arms are preferentially localized farthest way from the core. Whereas these *average* properties of a confined star and of a two-chain system nicely agree with those of a polymer brush, there are pronounced differences in the *fluctuations*. The geometrically confined systems exhibit bistability in the relative positions of the two arm ends residing on the same side of the core or in the two-chain system. Indeed, the probability of the difference of the end-positions, $z_1 - z_2$, has zero mean but is bimodal, indicating that the two free ends effectively repel each other. This observation is in qualitative contrast to the respective behavior in a polymer brush where the corresponding distribution is a Gaussian centered around zero. It highlights that fluctuation effects in nanoscale confinement, where one macromolecule interacts only with a few neighbors, may qualitatively differ from the mean-field picture.

AUTHOR INFORMATION

Corresponding Author

*(A.M.) E-mail: milchev@ipc.bas.bg.

Notes

The authors declare no competing financial interest.

ACKNOWLEDGMENTS

A.M. is indebted to the Georg-August University, Göttingen, Germany, and to the European Commission for hospitality and financial support under Grant No. PITN-GA-2008-214919 (MULTIFLOW) during part of this study. L.K. acknowledges financial support by the Deutsche Forschungsgemeinschaft (Grant SCHM 985/13-1)

REFERENCES

(1) Milner, S. T.; McLeish, T. C. B. *Macromolecules* **1997**, *30*, 2159.
(2) Grest, G. S.; Fetters, L. J.; Huang, J. S.; Richter, D. *Adv. Chem. Phys.* **1996**, *94*, 67.
(3) Qui, L. Y.; Bae, Y. H. *Pharm. Res.* **2006**, *23*, 1.
(4) Wiltshire, J. T.; Qiao, G. G. *Aust. J. Chem.* **2007**, *60*, 699.
(5) Gao, H. *Macromol. Rapid Commun.* **2012**, *33*, 722.
(6) Frischknecht, A. L.; Milner, S. T. *Macromolecules* **2000**, *33*, 9764−9768.
(7) Frischknecht, A. L.; Milner, S. T.; Pryke, A.; Young, R. N.; Hawkins, R.; McLeish, T. C. B. *Macromolecules* **2002**, *25*, 4801−4820.
(8) Ngai, K. L.; Roland, C. M. *J. Polym. Sci., Part B* **1997**, *35*, 2503−2510.
(9) Colley, F. R.; Collins, S. A.; Richards, R. W. *J. Mater. Chem.* **2003**, *13*, 2765−2770.
(10) Vega, D. A.; Gomez, L. R.; Roth, L. E.; Ressia, J. A.; Villar, M. A.; Valles, E. M. *Phys. Rev. Lett.* **2005**, *95*, 16602.
(11) Truzzolillo, D.; Vlassopoulos, D.; Gauthier, M. *Macromolecules* **2011**, *44*, 5043−5052.
(12) Bartels, C. R.; Crist, B., Jr.; Fetters, L. J.; Grassley, W. *Macromolecules* **1986**, *19*, 785.
(13) Pearson, D. S.; Helfand, E. *Macromolecules* **1984**, *17*, 888.
(14) Milner, S. T.; McLeish, T. C. B. *Macromolecules* **1997**, *30*, 2159−2166.
(15) Milner, S. T.; McLeish, T. C. B. *Macromolecules* **1998**, *31*, 7479−7482.
(16) de Gennes, P.-G. *J. Phys. (Paris)* **1975**, *36*, 1199.
(17) Camargo, M.; Egorov, S. A.; Likos, C. *Soft Matter* **2012**, *8*, 4177−4184.
(18) Mayer, C.; Likos, C. *Macromolecules* **2007**, *40*, 1196−1206.
(19) Likos, C. N.; Löwen, H.; Watzlawek, M.; Abbas, B.; Jucknischke, O.; Allgaier, J.; Richter, D. *Phys. Rev. Lett.* **1998**, *80*, 4450−4453.
(20) Grest, G. S.; Kremer, K.; Witten, T. A. *Macromolecules* **1987**, *20*, 1376−1383.
(21) Singh, S. P.; Fedosov, D. A.; Chatterji, A.; Winkler, R. G.; Gompper, G. *J. Phys.: Condens. Matter* **2012**, *24*, 464103.
(22) Gao, J.; Luedtke, W. D.; Landman, U. *J. Chem. Phys.* **1997**, *106*, 4309−4318.
(23) Sikorski, A.; Kolinski, A.; Skolnick, J. *Macromol. Theory Simul.* **1994**, *3*, 715−729.
(24) Brown, S.; Szamel, G. *Macromol. Theory Simul.* **2000**, *9*, 14−19.
(25) Di Cecca, A.; Freire, J. J. *Polymer* **2003**, *44*, 2589−2597.
(26) Grest, G. S.; Kremer, K. *Phys. Rev. A* **1986**, *33*, 3628.
(27) Romiszowski, P.; Sikorski, A. *J. Mol. Model.* **2009**, *15*, 681−686.
(28) Halperin, A.; Alexander, S. *Macromolecules* **1987**, *20*, 1146−1152.
(29) Sevick, E. M. *Macromolecules* **2000**, *33*, 5743−5746.
(30) Maury-Evertz, J. R.; Estevez, L. A. *J. Chem. Phys.* **2004**, *121*, 8652−8657.
(31) Lau, H. W.; Archer, L. A. *Phys. Rev. E* **2011**, *84*, 061916.
(32) Romiszowski, P.; Sikorski, A. *J. Phys. Chem.* **2002**, *116*, 1731−1736; *J. Phys. Chem.* **2004**, *120*, 7206−7211.
(33) Romiszowski, P.; Sikorski, A. *J. Phys.-Condens. Matter* **2007**, *19*, 205136.
(34) Romiszowski, P.; Sikorski, A. *Comp. Methods Sci. Technol.* **2012**, *18*, 39−44.
(35) Paturej, A.; Milchev, A.; Egorov, S. A.; Binder, K. *Soft Matter* **2013**, *9*, 10522.
(36) Sakaue, T.; Raphaël, E.; de Gennes, P.-G.; Brochard-Wyart, F. *Europhys. Lett.* **2005**, *72*, 83−88.
(37) Ge, H.; Pispas, S.; Wu, C. *Polym. Chem.* **2011**, *2*, 1071.
(38) Zhang, Y.; de Pablo, J. J.; Graham, M. D. *Soft Matter* **2009**, *5*, 3694−3700.
(39) Osmanovic, D.; Bailey, J.; Harker, A. H.; Fassati, A.; Hoogenboom, B. W.; Ford, I. J. *Phys. Rev. E* **2012**, *85*, 061917.
(40) Arnold, A.; Bozorgui, B.; Frenkel, D. *J. Chem. Phys.* **2007**, *127*, 164903.
(41) Arnold, A.; Jun, S. *Phys. Rev. E* **2007**, *76*, 031901.
(42) Ibanez-Garcia, G. O.; Goldstein-Menache, P. *Soft Matter* **2012**, DOI: 10.1039/c2sm25257k.
(43) Jung, Y.; Ha, B.-Y. *Phys. Rev. E* **2010**, *82*, 051926.
(44) des Cloizeaux, J. *J. Phys. (Paris)* **1975**, *36*, 281.
(45) de Gennes, P.-G. *Adv. Polym. Sci.* **1999**, *138*, 91−105.
(46) Pincus, P. *Macromolecules* **1976**, *9*, 386.
(47) Hsu, H.-P.; Binder, K.; Klushin, L. I.; Skvortsov, A. M. *Phys. Rev. E* **2007**, *76*, 021108.
(48) Freed, K. F.; Wu, C. *J. Chem. Phys.* **2001**, *135*, 144902.
(49) Livadaru, L.; Kreuzer, H. J. *New J. Phys.* **2003**, *5*, 95.195.18.
(50) Milchev, A.; Paul, W.; Binder, K. *Macromol. Theory Simul.* **1994**, *3*, 305−323.
(51) de Gennes, P.-G. In *Scaling concepts in polymer physics*; Cornell University Press: Ithaca, NY, 1985.
(52) Milchev, A.; Paul, W.; Binder, K. *J. Chem. Phys.* **1993**, *99*, 4786.
(53) Milchev, A.; Binder, K. *Macromol. Theory Simul.* **1994**, *3*, 915.
(54) Milchev, A.; Binder, K. *Macromolecules* **1996**, *29*, 341.
(55) Milchev, A.; Binder, K. *J. Chem. Phys.* **2001**, *114*, 8610.
(56) Binder, K. *Rep. Prog. Phys.* **1997**, *60*, 487.

(57) Kreer, T.; Metzger, S.; Müller, M.; Binder, K.; Baschnagel, J. *J. Chem. Phys.* **2004**, *120*, 4012.
(58) Semenov, A. N. *Sov. Phys. JETP Lett.* **1985**, *61*, 733.
(59) Alexander, S. *J. Phys. (Fr.)* **1977**, *38*, 983.
(60) Müller, M.; Binder, K.; Schäfer, L. *Macromolecules* **2000**, *33*, 4568−4580.
(61) Merlitz, H.; He, G.-L.; Wu, C.-X.; Sommer, J.-U. *Phys. Rev. Lett.* **2009**, *102*, 115702.
(62) Müller, M.; Schmid, F. *Adv. Polym. Sci.* **2005**, *185*, 1−58.
(63) Risken, H. *The Fokker-Planck equation: Methods of Solutions and Applications*; Springer: Berlin, 1989.
(64) Redner, S. *A Guide to First-Passage Processes*: Cambridge University Press: 2001; Section 2.2, p 49, eq 2.2.26.
(65) Gardiner, C. *Stochastic methods*; Springer: Berlin, 2010.
(66) Masubuchi, Y.; Ianniruberto, G.; Greco, F.; Marucci, G. *Rheol. Acta* **2006**, *46*, 297−303.
(67) Masubuchi, Y.; Yaoita, T.; Matsumiya, Y.; Watanabe, H. *J. Chem. Phys.* **2011**, *134*, 194905.
(68) Shanbhag, S.; Larson, R. G. *Macromolecules* **2004**, *37*, 8160−8166.